Seaward expansion of salt marshes maintains morphological self-similarity of tidal channel networks

Seaward expansion of salt marshes maintains morphological self-similarity of tidal channel networks

Zhicheng Yang[1], Alvise Finotello[1], Guillaume Goodwin[2,3,9], Chao Gao[1,4], Simon M. Mudd[3], Dimitri Lague[5], Christian Schwarz[6,7], Bo Tian[8], Massimiliano Ghinassi[1], Andrea D'Alpaos[1]*

[1] *Department of Geosciences, University of Padova, Padova, Italy*

[2] *Department of Civil, Environmental and Architectural Engineering, University of Padova, Padova, Italy*

[3] *School of GeoSciences, University of Edinburgh, Edinburgh, UK*

[4] *Ministry of Education Key Laboratory for Coast and Island Development, School of Geographic and Oceanographic Sciences, Nanjing University, Nanjing, China*

[5] *CNRS, Géosciences Rennes, University of Rennes, Rennes, France*

[6] *Department of Civil Engineering, KU Leuven, Leuven, Belgium*

[7] *Department of Earth and Environmental Sciences, KU Leuven, Leuven, Belgium*

[8] *State Key Laboratory of Estuarine and Coastal Research, East China Normal University, 200062, Shanghai, China*

[9] *Fish-Pass, Laillé, France*

* Corresponding author: Andrea D'Alpaos (andrea.dalpaos@unipd.it)

Abstract

Tidal channel networks (TCNs) dissect ecologically and economically valuable salt marsh ecosystems. These networks evolve in response to complex interactions between hydrological, sedimentological, and ecological processes that act in tidal landscapes. Thus, improving current knowledge of the evolution of salt-marsh TCNs is critical to providing a better understanding of bio-morphodynamic processes in coastal environments. Existing studies of coastal TCNs have typically focussed on marshes with either laterally stable or eroding edges, and suggested that TCN morphology evolves primarily through the progressive landward erosion of channel tips, that is, *via* channel headward growth. In this study, we analyze for the first time the morphological evolution of TCNs found within salt marshes that are characterized by active lateral expansion along their seaward edges and anthropogenically-fixed landward boundaries. We use remote-sensing and numerical-modeling analyses to show that marsh seaward expansion effectively limits headward channel growth and prompts the evolution of TCNs that maintain self-similar morphological structures. In particular, we demonstrate that the overall TCN length increases proportionally to the rate at which marshes expand laterally and that these morphological changes do not significantly alter the drainage properties of the coupled marsh-TCN system. Such behavior is not observed in marshes that are not expanding laterally. Our results allow for elucidating the mechanisms of TCN formation and evolution in tidal wetlands, and are therefore critical to improving our current understanding of coastal-landscape ecomorphodynamics, as well as to developing sustainable strategies for the conservation and restoration of these environments.

***Keywords**: tidal channel networks; lateral expansion salt marshes; self-similarity; drainage properties.*

Highlights:

- The evolution of tidal networks (TCNs) in laterally-expanding salt marshes is analyzed
- TCNs maintain morphological self-similarity as marshes expand seaward
- Self-similarity is not maintained in eroding marshes where TCNs evolve via headward growth

1. Introduction

Tidal channel networks (TCNs) are widespread geomorphological features in tidal saline wetlands (Cleveringa & Oost, 1999; Coco et al., 2013; D'Alpaos et al., 2005, 2007; Feola et al., 2005; Schwarz et al., 2022; Shi et al., 1995). TCNs form the main paths for the exchange of water, sediments, nutrients, and energy between tidal wetlands and open waters, thus exerting a fundamental control on the ecomorphodynamic evolution of these coastal ecosystems (Kearney & Fagherazzi, 2016; Sanderson et al., 2000, 2001). The morphological evolution of TCN planform morphology is typically driven by channel headward growth, a mechanism whereby channels extend landward via the progressive carving of their tips (e.g., Allen, 2000; Coco et al., 2013; D'Alpaos et al., 2005; Feola et al., 2005; Hughes et al., 2009), with second-order adjustments due to lateral migration of individual channels (Cosma et al., 2020; D'Alpaos et al., 2017; Finotello et al., 2018; Jarriel et al., 2021). Such a head-cutting mechanism depends on the spatial distribution of tidal-current-induced bottom shear

stresses, the largest values of which are typically found around channel tips as a consequence of the characteristic hydrodynamic fields generated by tidal level fluctuations across frictionally-dominated intertidal platforms (D'Alpaos et al., 2005, 2021). The importance of headward growth for TCN evolution has been highlighted by both laboratory and numerical experiments (Coco et al., 2013; D'Alpaos et al., 2005; Finotello et al., 2019; Geng et al., 2020; Kleinhans et al., 2012; Lentsch et al., 2018; Stefanon et al., 2012, 2010; Vlaswinkel and Cantelli, 2011; Zhou et al., 2014a, 2014b), with field studies suggesting variable rates of headward growth ranging from few centimeters to hundreds of meters per year (e.g., D'Alpaos et al., 2007; Flint, 1973; Hughes et al., 2009; Knighton et al., 1992, 1991; Leopold et al., 1993; May, 2002; Rankey and Morgan, 2002; Van Maanen et al., 2015; Vandenbruwaene et al., 2012)).

While headward growth has been typically documented either in TCNs that are still evolving and have not yet achieved a quasi-steady equilibrium or in mature wetland systems affected by rising relative sea level - a common condition in most coastal regions worldwide - empirical observations suggest that TCNs could also expand when tidal wetlands prograde seaward by colonizing adjoining unvegetated tidal flats (Chambers et al., 2003; Goodwin and Mudd, 2020; Kirwan et al., 2011; Ladd et al., 2019; Willemsen et al., 2022) (Fig. 1). Data regarding this latter morphodynamic process are however scarce, mostly because of the inherent tendency of tidal wetlands worldwide to retreat, rather than expand laterally, due to a lack of sufficient mineral sediment supply (Fitzgerald and Hughes, 2019; Roner et al., 2021; Willemsen et al., 2022; Yang et al., 2020). Therefore, it remains unclear how wetland lateral expansion affects the morphology and related ecosystem functioning of tidal channel

79 networks, and how these changes feedback into the hydrodynamics of the wetland ecosystem as a
80 whole.

81 Here we monitor the temporal evolution of TCN morphometric characteristics in a set of 6 laterally
82 expanding tidal salt marshes, each characterized by distinct tidal regimes and vegetation covers. We
83 focus specifically on the coupled evolution of marsh area and total TCN length, as well as on temporal
84 changes in marsh drainage density due to seaward network expansion (Marani et al., 2003; Tucker et
85 al., 2001). The latter is synthesized here by the distribution of drainage distance (Rinaldo et al., 1999a;
86 Tucker et al., 2001), that is, the distance that a water particle needs to travel on the marsh platform
87 before entering a nearby tidal channel (Marani et al., 2003a). Drainage density, defined as the inverse
88 of the mean drainage distance, is an indicator of the overall TCN efficiency in draining the marsh and
89 bears tight inherent associations to vegetation appearance and hydrodynamic processes in tidal
90 wetlands (Geng et al., 2021; Temmerman et al., 2007).

91 ## 2. Material and Methods

92 ### 2.1 Study cases and geomorphological settings

93 We investigated the spatio-temporal evolution of TCNs in six different salt-marsh systems worldwide,
94 each characterized by different marsh morphology, vegetation cover, and tidal range. All the studied
95 marshes are characterized by active expansion in the seaward direction during the considered time
96 periods. In contrast, the landward expansion of these systems is impeded by the presence, at the
97 landward marsh boundary, of man-made structures such as dikes and seawalls. A brief description of
98 each marsh is reported in the next paragraphs.

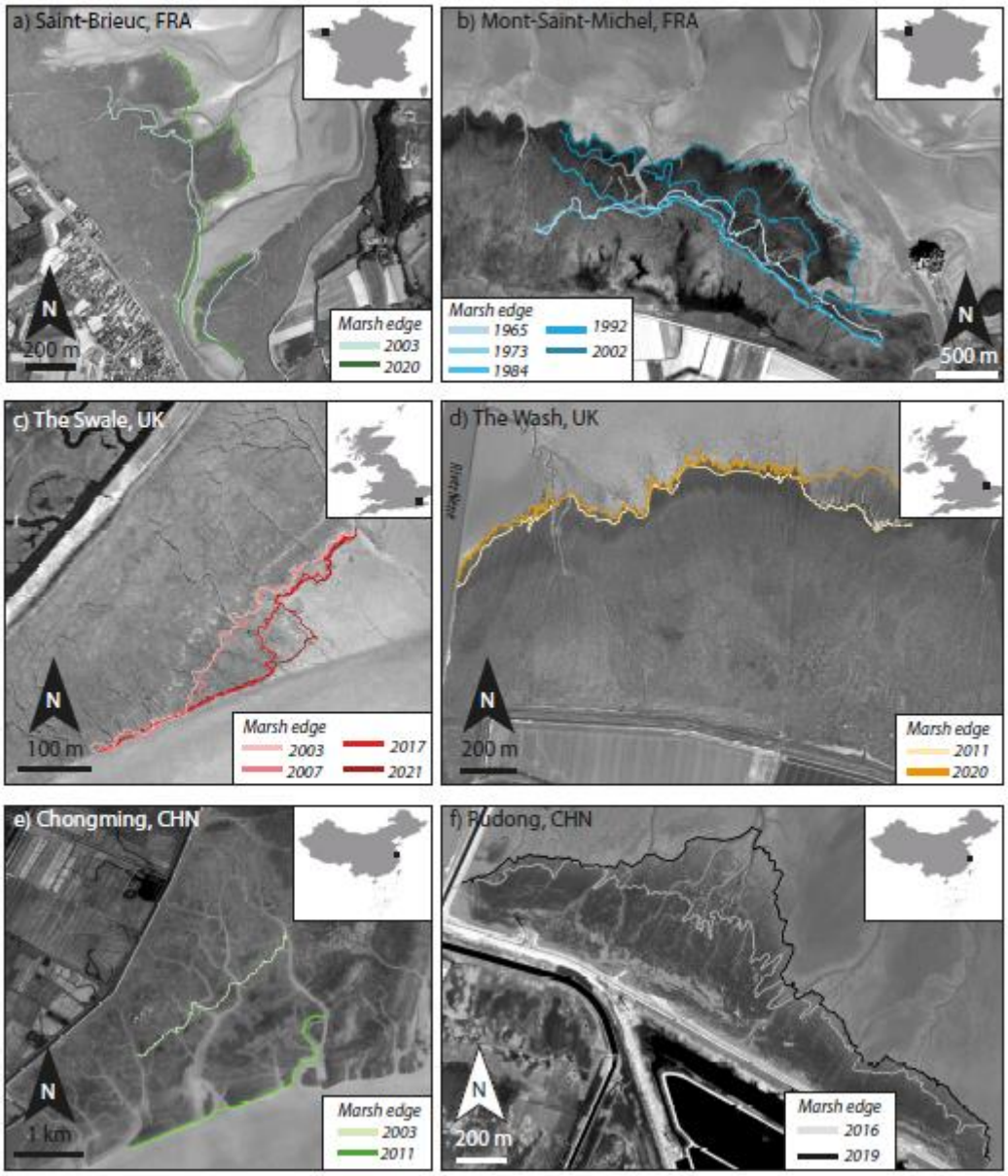

99

100 ***Fig. 1.*** *Aerial view and temporal evolution of marsh extent at the six study sites analyzed in the*
101 *present work. (a,b) Salt marshes in Saint-Brieuc (SB, Map data: Google, Maxar Technologies; 48°*
102 *30'N, 2° 41'W; date: 2020-05-31) and Mont Saint Michel (MSM, Map data: Google, Maxar*
103 *Technologies; 48° 38'N, 1° 33'W; date: 2003-04-19), France; (c,d) Salt marshes in the Swale (SW,*
104 *Map data: Google, Landsat; 51° 22'N, 0° 56'E; date: 2021-03-30) and the Wash (WS, Map data: UK*
105 *Department for Environment Food & Rural Affairs; 52° 49'N, 0° 13'E; date: 2020-06-01), United*

Kingdom; (e,f) Salt marshes in Chongming (CM, Map data: Formosat 2, 31° 28'N, 121° 57'E) and Rudong (RD, Map data: Google, CNES, 32° 33'N, 121° 7'E; date: 2019-03-07), People's Republic of China. Locations of the marsh seaward margins in different years are shown for each study case according to the legend displayed in each panel.

The first two study cases consist of salt marshes found in Saint Brieuc bay and Mont Saint Michel bay, both located in northwestern France (Figure 1a,b).

The Saint-Brieuc bay (SB, 48° 30'N, 2° 41'W, Fig 1a) is an open bay characterized by a semi-diurnal macrotidal regime, with neap and spring tides of 4 and 13 m, respectively (Sturbois et al., 2021). Fringing marshes extend seaward by encroaching tidal flats and cannot extend landward due to the construction of seawalls (Fig. 1a). The study site is an estuarine marsh located on the upper shore that currently covers an area of about 1.25 km^2 in total (Sturbois et al., 2022). The marsh has exhibited active seaward expansion over the last 50 years. The upper marsh portions are dominated by *Halimione portulacoides*, whereas the lower marsh is mainly colonized by *Salicornia spp* (Ponsero et al., 2009). Changes in TCN structure and the related geometric features in this area were analyzed by means of two aerial images taken in 2003 (©Google, Landsat) and 2020 (©Google, Maxar), respectively, both accessed through Google Earth Pro. Visual observation of historical images suggests that, during the investigated period, the western portions of the marsh (SB-West) underwent faster seaward expansion relative to the marsh located in the eastern part of the system (SB-East; see Fig. 1a and Fig. 2a,b). Specifically, marsh expansion rates in SB-West and SB-East over the considered period (Fig. 2c,f) amount to 6.47×10^{-3} and 9.47×10^{-4} km^2/year, respectively. Since SB-West and SB-East expanded seaward with opposite compass directions (i.e., the western marsh

127 portion expanded eastward, whereas the eastern portion expanded westward), marshes and TCNs in
128 each area were analyzed separately (Fig. 2a,b,d,e).

129 The Mont Saint Michel bay (MSM, Fig. 1b) is a 500 km^2 open bay located on the northwest coast of
130 France, between Brittany and the Cotentin Peninsula (Furgerot et al., 2016; Tessier et al., 2012). The
131 Bay is affected by a semi-diurnal hypertidal regime (Desguée et al., 2011; Détriché et al., 2011), and
132 with maximum spring tidal ranges larger than 13 m it witnesses the second largest tidal range in
133 Europe (Levoy et al., 2017, 2000). Sediment grain size decreases from the lower part of the tidal flats
134 to the upper part, indicating that wave energy reduces progressively in the landward direction (Levoy
135 et al., 2017). The lower and mid-intertidal zones mainly comprise medium to fine sands, whereas the
136 upper intertidal zone is characterized by very fine bio-clastic sand (Desguée et al., 2011). Mud content
137 ranges from 20 to 25% in the proximity of salt-marsh platforms, and is even higher within salt
138 marshes (Levoy et al., 2017). Our study area consists of an expanding (5.0×10^{-2} km^2 between 1973
139 and 2002), non-grazed salt marsh located in the western portion of the MSM (Fig. 1b). Marshes here
140 are mainly dominated by four halophytic species: *Hallimoniae portulacoides*, *Spartina anglica*,
141 *Suaeda maritima*, and *Puccinellia Maritima.* The evolution of TCNs in MSM was analyzed through a
142 temporal series of aerial imageries, dating back to 1965 and spanning about 40 years (i.e., 1965, 1973,
143 1984, 1992, and 2002), with spatial resolutions ranging from 0.44 to 0.94 m.

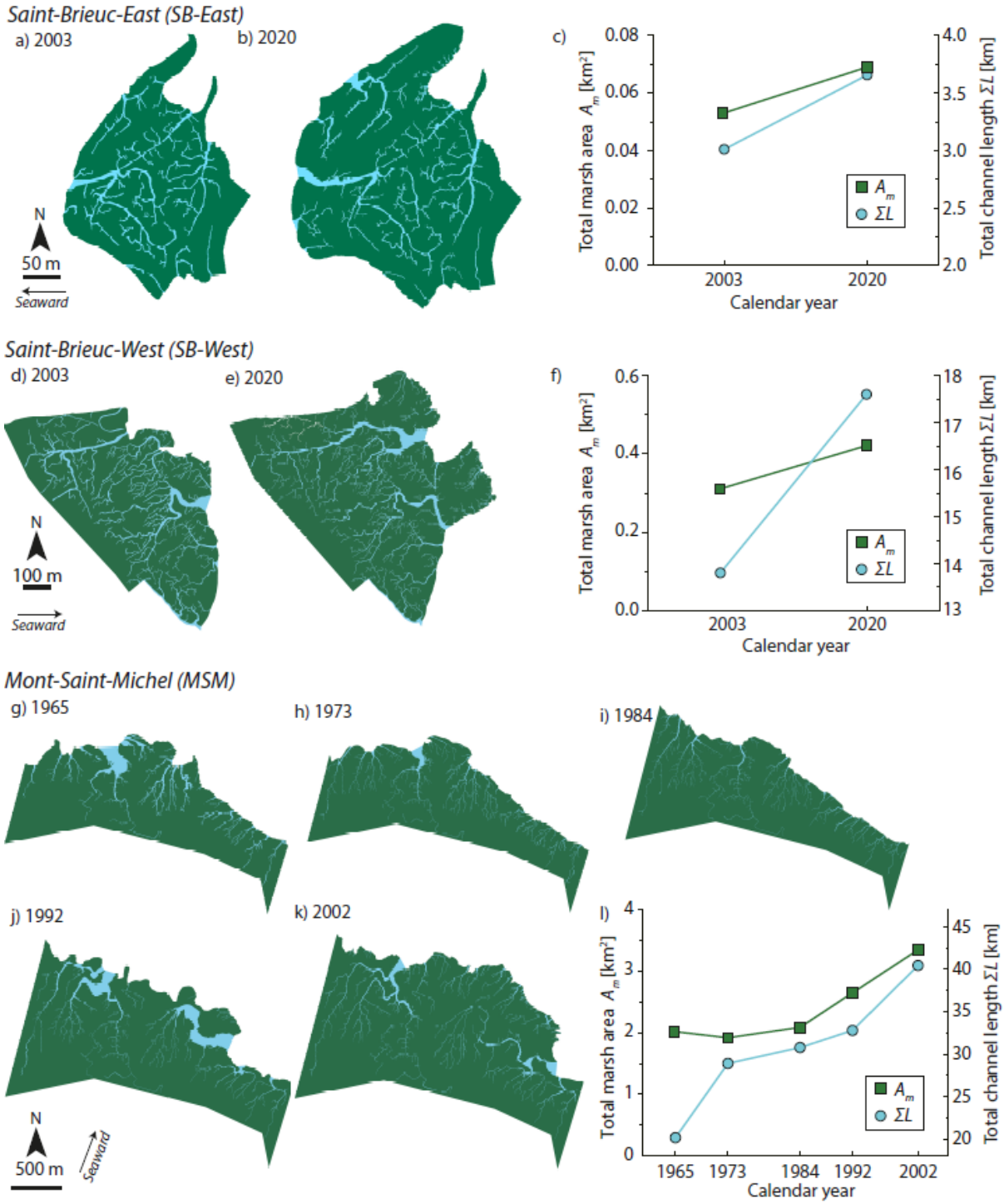

144

145 ***Fig. 2.*** *Binary maps of marsh-channel systems for the study cases located in France. (a,b) Binary*

146 *maps of the Saint Brieuc East (SB-East) marsh in 2003 and 2020; (c) Changes in total marsh area*

147 *(A_m, green, left y-axis) and total channel length ($\sum L$, cyan, right y-axis) through time in SB-East; (d,e)*

148 *Binary maps of the Saint Brieuc West (SB-West) marsh in 2003 and 2020; (f) Changes in total marsh*

area (A_m, green, left y-axis) and total channel length ($\sum L$, cyan, right y-axis) through time in SB-West; (g,h,I,j,k) Binary maps of the Mont Saint Michel (MSM) marsh in 1965,1973,1984, 1992, and 2002; (l) Changes in total marsh area (A_m, green, left y-axis) and total channel length ($\sum L$, cyan, right y-axis) through time in MSM.

The two further study cases are found on the southeastern coasts of the UK. Specifically, we analyzed two salt marshes found within the Swale estuary and the Wash tidal bay (Fig.1c,d). The Swale (SW; 51° 22'N, 0° 56'E; Fig. 1c) is a tidal channel of the Thames River estuary that separates the Isle of Sheppey from the rest of Kent. The selected marsh is located at the southeastern end of the Isle of Sheppey (Fig. 1c), and is characterized by a semidiurnal macrotidal regime with a spring tidal range of about 5.2 m (Spencer et al., 2003; van der Wal and Pye, 2004). This area is dominated by fine, muddy sediments (Cundy et al., 2007). This marsh is mainly populated by *Polygonum, Crambe maritima*, glassworts, and *Limbarda crithmoides*. The studied marsh is separated from the reclaimed Swale National Nature Reserve by artificial dikes, which effectively prevent marshes from migrating landward. Visual inspections of historical maps available on Google Earth Pro suggest that the marsh analyzed in this study is characterized by the most pronounced expansion rate in the area. Specifically, between 2007 and 2021 (Fig. 3b-d), the marsh expanded at a rate of about 8.94×10^{-4} km^2/year, after a period of relative stability (2003-2007; Fig. 3a-b) during which the total marsh area remained stable at about 1.04×10^{-2} km^2. Variations in TCN geometry in the SW in the last 20 years were explored through the analysis of a temporal series of aerial photographs, consisting of imagery scenes acquired by Infoterra Ltd & Bluesky (©Google) in 2003 and 2007, and by Landsat (©Google) in 2017 and 2021, all of which were accessed through Google Earth Pro.

The Wash estuary (WS; 52° 49'N, 0° 13'E; Fig. 1d) is located in eastern England (Pye, 1995). The tidal regime is semidiurnal macrotidal (Ni et al., 2014), with a spring tidal range approximately equal to 6.5 m (Cahoon et al., 2000; Goudie, 2013). Marshes in the Wash have been characterized by significant rates of seaward expansion (1.27×10^{-2} km^2/year) and vertical accretion (46.17 mm/year) in the last decades (Ladd et al., 2019). Marsh surface is typically encroached by *Puccinellia maritima*, *Halimione portulcoides,* and *Elymus pycnanthus* (Norris et al., 1997). Sediments consist mostly of silt and clay (Pye, 1995). About 30% of marshes in the Wash are still grazed, mainly by cattle, sheep, and horses (Norris et al., 1997). The marsh portion analyzed here is located in the southern area of the estuary, eastern of the mouth of River Nene, where man-made embankments built at the marsh landward boundaries (Ni et al., 2014) do not allow for the marsh to migrate landward. Changes in TCN within the studied area were analyzed, from 2011 to 2020, based on multi-spectral data with a spatial resolution equal to 0.20 m that are freely available from the UK Department of Environment, Food, and Rural Affairs (DEFRA) data service platform. During the considered period, the marsh expanded seaward at a rate of about 8.2×10^{-3} km^2/year.

Finally, two actively-expanding salt marshes were identified along the coast of China. The first one is represented by a salt marsh found on the Chongming Island (CM; 31° 28'N, 121° 57'E), within the Yangtze Estuary (China; Fig. 1e). The tidal regime in CM is semidiurnal meso- to macro-tidal, with an average tidal range of about 2.5 m reaching up to 3.5 m during spring tides (Shi et al., 2012). Due to the abundant sediment availability provided by the Yangtze River, in the last decades, the marsh has rapidly extended seaward at rates of about 150-300 m/year and accreted vertically with an average rate of about 50 mm/year (Yang et al., 2011, 2005). The main halophytic vegetation species here are

191 *Scirpus mariqueter*, *Phragmites australis*, and *Spartina alterniflora* (Zhao et al., 2019). The
192 morphometry of local TCNs is analyzed by using 2 satellite images acquired in 2003 (IKONOS) and
193 2011 (Formosat 2) (Chen et al., 2021). Both IKONOS and Formosat 2 are multi-spectral sensors, and
194 their spatial resolutions are 1 and 2 m, respectively.

195 The second studied marsh is instead found in Rudong (RD, Fig. 1f), located in the middle sector of the
196 Jiangsu coast. This marsh has significantly prograded seaward (6.6×10^{-2} km^2/year) in the last
197 decades, thanks to active sediment supply from the Subei Coastal Current and nearshore residual
198 currents influenced by the abandoned Yellow River Delta (Li et al., 2018). The tidal regime in Rudong
199 is semidiurnal macrotidal, with an average tidal range of about 4.5 m (Wang et al., 2012). The studied
200 marsh is dominated by native communities composed of *Phragmites australis*, *Suaeda*
201 *glauca*, *Imperata cylindrical*, and invasive species *Spartina alterniflora* (Li et al., 2018). Field
202 observations suggest that local sediments mainly consist of silt, with smaller fractions of sand and
203 clay (Yang et al., 2021). Dikes have been constructed at the marsh landward boundaries, thus
204 preventing marshes from migrating landward. Changes in TCN morphology between 2016 and 2019
205 were analyzed by using aerial imageries (©Google, Maxar Technologies) accessed from Google Earth
206 Pro.

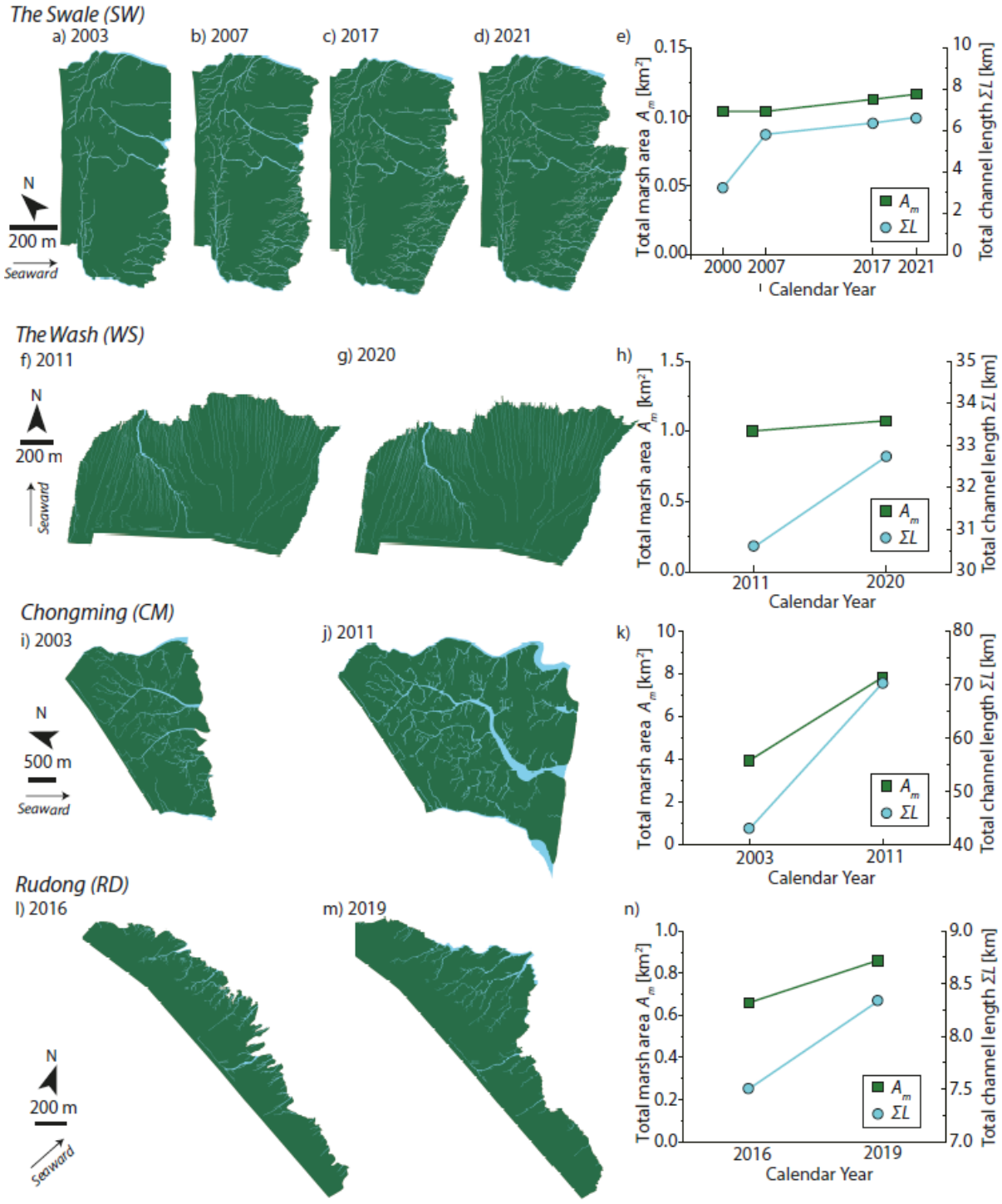

207

208 ***Fig. 3.*** *Binary maps of marsh-channel systems for the study cases located in the United Kingdom and*

209 *China. (a,b,c,d) Binary maps of the Swale (SW) marsh in 2003, 2007, 2017, and 2021; (e) Changes in*

210 *total marsh area (A_m, green, left y-axis) and total channel length ($\sum L$, cyan, right y-axis) through*

211 *time in SW; (f,g) Binary maps of the Wash (WS) marsh in 2011 and 2020; (h) Changes in total marsh*

area (A_m, green, left y-axis) and total channel length ($\sum L$, cyan, right y-axis) through time in WS; (i,j) Binary maps of the Chongming (CM) marsh in 2003 and 2011; (k) Changes in total marsh area (A_m, green, left y-axis) and total channel length ($\sum L$, cyan, right y-axis) through time in CM; (l,m) Binary maps of the Rudong (RD) marsh in 2016 and 2019; (k) Changes in total marsh area (A_m, green, left y-axis) and total channel length ($\sum L$, cyan, right y-axis) through time in RD.

2.2 Network extraction and morphometric analyses

Temporal variations in TCN morphology were analyzed based on the boundaries of both tidal-channel and salt-marsh edges extracted from the available remote sensing products. The position of channel banks and marsh margins were hand digitized in ©ArcGIS 10.8 based on vegetation cover and locations of seawalls and dikes. We adopted manual digitization because, although labor intensive, it is generally more precise than pixel- and object-based classification procedures, especially when dealing with minor channels whose width is comparable to image resolution (e.g., Kalkan et al., 2013). After manual digitization, channel networks and marsh boundaries were then converted into binary maps of marsh-channel area by using ©Arcmap 10.8 (Figs. 2 and 3). Based on such binary maps, we first estimated the overall area of the marsh (A_m) and channel portions (A_c). Then, by applying a skeletonization procedure (Kerschnitzki et al., 2013) in ©Matlab R2020a to the channel portions of the maps, we derived the centerlines of individual tidal channels, from which the total length of the TCN ($\sum L$) was estimated. In addition, based on the computed binary maps, we also calculated and analyzed the temporal evolution of TCN drainage density (Marani et al., 2003) taking advantage of the drainage directions determined by applying the simplified intertidal hydrodynamic model proposed by Rinaldo et al. (1999a). The model solves a linearized version of the shallow-water

equations, suitably simplified to reduce computational expense while maintaining the description of the main characteristics of the hydrodynamic circulation in intertidal, frictionally-dominated settings (Rinaldo et al., 1999a, 1999b; Marani et al., 2003). In detail, assuming that the slope of the water-free surface is in equilibrium with the energy dissipations, the shallow water equations can be simplified as follows:

$$\nabla\eta_1 = -\frac{\lambda}{D}\boldsymbol{U} \quad (1)$$

where $\eta_1(\boldsymbol{x}, t)$ represents the local deviation of the free surface elevation from its mean instantaneous value $\eta_0(t)$ relative to the mean sea level ($\boldsymbol{x}$ indicates the coordinate vector, whereas t is time), $\boldsymbol{U}(\boldsymbol{x}, t)$ is the local depth-integrated flow velocity, $D = \eta_0 + \eta_1 - z_b$ is the local water depth relative to the bottom elevation z_b, and λ is a spatially-constant bottom friction coefficient that depends both on the Chezy's parameter (χ) and the maximum characteristic value of the velocity over the marsh surface (U_{MAX}) according to the relation (Rinaldo et al., 1999a):

$$\lambda = 8 \cdot \frac{U_{max}}{3\pi \cdot \chi^2} \quad (2)$$

We assumed χ=10 $m^{1/2}/s$ and U_{MAX}=0.2 m/s, consistent with the approach proposed by Rinaldo et al. (1999a) and Marani et al. (2003a). By substituting the previous equations within the continuity equation, and further assuming that the tide propagates instantaneously within the tidal channel network (i.e., η_1=0 within channels) and imposing zero flux along the impermeable edges of the domain (i.e., $\partial\eta_1/\partial n$=0, with n being the direction normal to the domain boundary), it is possible to determine the instantaneous free-surface elevation along the un-channeled marsh surface by solving the following Poisson problem:

$$\nabla^2\eta_1 = \frac{\lambda}{D_0^2}\left(\frac{\partial\eta_0}{\partial t}\right) = k \quad (3)$$

where D_0 denotes the average water depth over the entire marsh domain. After solving equation (3) for an arbitrary tidal forcing (i.e., given values of both D_0 and η_0, where $d\eta_0/dt$ is the rate of change in the water level in the estuary and is determined by the tide), time-independent flow directions at any location within the intertidal domain are computed as the time-invariant, steepest-descent direction of the water surface elevation. Then, the drainage distance at any marsh location can be determined as the distance (ℓ) that a water particle has to travel to reach the closest channel edge following the flow directions. The drainage density of the tidal landscape can be eventually defined based on the probability distribution of ℓ computed for the whole unchanneled marsh domain (e.g., Feola et al., 2005; Marani et al., 2003; Zeng Zhou et al., 2014b). Previous analyses suggest that such probability distribution follows an exponential trend (D'Alpaos et al., 2005; Feola et al., 2005; Marani et al., 2003a; Zhou et al., 2014). Thus, the exceedance probability of drainage distance (i.e., $P(L > \ell)$) plotted in a semi-log diagram should display a sublinear trend, jointly with the finite-size scaling effect induced by the cutoff dictated by the site-specific maximum value of ℓ. Therefore, the mean drainage distance (ℓ_m) can be computed as the inverse slope of the linear portion of $P(L > \ell)$, which is easily computed through least-square regression. Then, the characteristic marsh drainage density (δ) can be derived as the inverse of ℓ_m, that is, $\delta = \ell_m^{-1}$. Notably, the calculation of the water surface distribution also allows one to compute the bottom shear stress (τ) acting on the marsh platform, which reads:

$$\tau = -\gamma D\nabla\eta_1 \cong -\gamma(\eta_0 - z_0)\nabla\eta_1 \quad (4)$$

where γ is the specific weight of water, *D* is the local water depth, and $\nabla\eta_1$ is the local slope of water free surface. In order to estimate for each study case the distribution of the maximum bottom shear stresses (τ_{max}), a critical parameter to assess the tendency of TCNs to extend landward via headward growth, we assigned values of η_0 based on the characteristic spring tidal forcings (i.e., maximum tidal amplitude and period), whereas estimates of z_0 (i.e., the average marsh elevation relative to the mean sea level) were derived from literature data. The complete set of values adopted to compute τ_{max} is reported in Table 1.

Table 1. *Input values used to calculate the maximum bottom shear stress (τ_{max}) at each study site (SB: Saint Brieuc; MSM: Mont Saint Michel; SW: The Swale; WS: The Wash; CM: Chongming; RD: Rudong).*

Study case	**Spring tidal amplitude η_0 [m]**	**Mean marsh elevation z_0 [m a.m.s.l.]**	**Reference**
SB	6.50	5.5	Sturbois et al. (2021); Sturbois et al. (2022)
MSM	6.58	5.6	Desguée et al. (2011); Marjoribanks et al. (2019)
SW	2.80	2.4	Spencer et al. (2003); van der Wal and Pye (2004)
WS	3.30	3.0	Cahoon et al. (2000); Goudie (2013)
CM	1.80	1.6	Shi et al. (2012)
RD	2.20	1.3	Wang et al. (2012)

3. Results and Discussion

Binary maps of marsh-channel systems highlight that morphological changes occurred mostly through lateral expansion of the marsh seaward margins, since landward marsh migration was impeded by man-made dikes and seawalls, and the TCNs in our study typically did not exhibit significant

288 headward growth (Figs. 2 and 3, Table 2). Only two exceptions to this trend are found, represented by
289 marshes in MSM, where the overall marsh area slightly reduced between 1965 and 1973 at a rate of
290 about 1.88×10^{-2} km^2/year (Fig. 2g,h,l; see also Table 2), and SW, where marsh area slightly shrunk
291 between 2003 and 2007 at a rate of about 2.79×10^{-5} km^2/year (Fig. 3a,b,e; see also Table 2).

292 In all study cases, the total channel length ($\sum L$) increased over the monitored period, with data from
293 MSM and SW, for which more than two aerial scenes were available, suggesting varying rates of $\sum L$
294 increase through time (Figs. 2l and 3e). Binary marsh-channel maps (Figs. 2 and 3) suggest that active
295 headward growth of tidal channels occurred both in MSM between 1965 and 1973 (Fig. 2g,h) and in
296 SW between 2003 and 2007 (Fig. 3a, b), when $\sum L$ increased despite an overall reduction in marsh A_m
297 (Fig. 2l and 3e). In contrast, during periods of marsh lateral expansion, the position of channel tips did
298 not change significantly, and channels extended seaward accompanying progradation of the marsh
299 margins (Figs 2c,f,l and Fig. 3e,h,k,n). The coupled increase in channel length ($\sum L$) and total marsh
300 area (A_m) associated with relatively stable channel tips suggests that TCNs evolved predominantly *via*
301 seaward extension, rather than by headward erosion of channel endpoints.

302 The analysis of the relation between A_m and $\sum L$ demonstrates a significant correlation between marsh
303 area and channel length, which seems to hold even when marshes expand seaward and channels
304 lengthen predominantly by the progradation of their inlet positions (Fig. 4a). Similarly, a significant
305 correlation is also found between the total marsh area (A_m) and the total channel area (A_c) (Fig. 4b).
306 Moreover, our data highlight that the relative changes in total TCN length ($\Delta_{\sum L}$) are significantly
307 correlated to changes in the overall marsh area (Δ_{A_m}; $p < 0.01$ for the *t*- statistic of the hypothesis test
308 that the regression coefficient is equal to zero, see Fig. 4c), suggesting the morphological relationship

between the rate at which channels lengthen and marsh area increases can be approximated as linear. We speculate that this behavior might be different from that of TCNs evolving through headward erosion of channel tips on marshes with stable seaward and landward boundaries, wherein changes in $\sum L$ might occur irrespective of variations in A_m. To substantiate this claim, we compared the trend observed in $\Delta_{\sum L}$ vs. Δ_{A_m} data during periods of marsh seaward expansion with data derived from marshes characterized by relatively stable A_m and documented headward growth of channels (i.e., MSM in 1965-1973 and SW in 2003-2007). Furthermore, we also simulated the headward growth of TCNs numerically for all the study cases by increasing channel length through headward growth, without modifying the total marsh area. Specifically, we increased $\sum L$ by 10 to 20% according to the numerically-simulated distribution of τ_{max}. We simulated this by eroding channel tips with a probability proportional to the maximum local bottom shear stress computed by means of the hydrodynamic model (see Equation 4). Both field and simulated data (Fig. 4c) suggest that the headward growth of TCN produces patterns of $\Delta_{\sum L}$ vs. Δ_{A_m} that are statistically different from those we observed in seaward-expanding salt marshes. Hence, the functional linear relationship between $\Delta_{\sum L}$ and Δ_{A_m} that emerges from our data can be considered specific to the coupled TCN-marsh evolution in salt marshes actively undergoing seaward expansion.

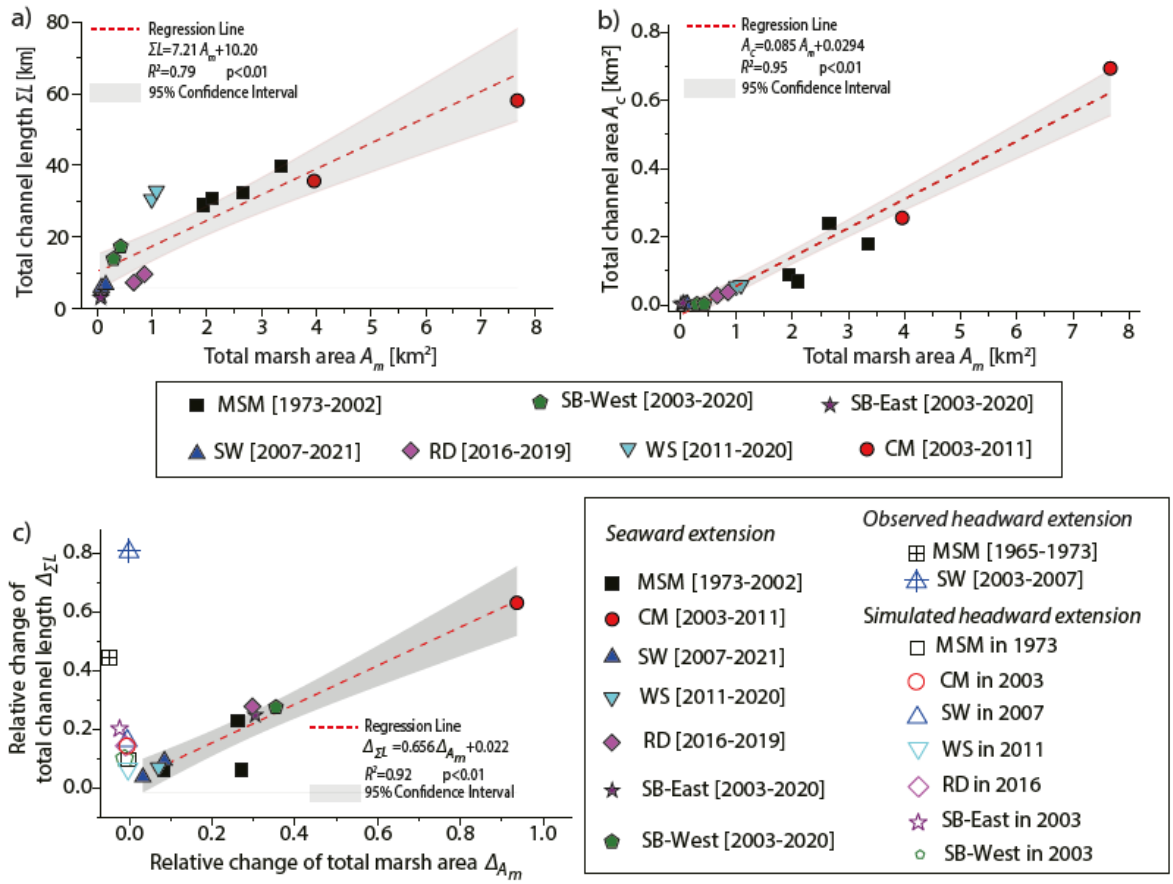

Fig. 4. *Morphometric relationships between salt-marsh and tidal-network features. (a,b) Plots of total marsh area (A_m) vs. total channel length ($\sum L$) and total channel area (A_c) for all the analyzed study cases. Results of linear regression analyses, together with correlation coefficients, p-values, and 95% confidence interval of the regression models are also reported. (c) Plot of relative change in total marsh area (Δ_{A_m}) vs. relative change in total channel length ($\Delta_{\sum L}$). Filled markers denote data retrieved from salt marshes undergoing active lateral expansion in the seaward direction, whereas empty markers highlight field and numerical data from laterally-stable or retreating marshes. Results of linear regression analyses, together with correlation coefficients, p-values, and 95% confidence interval of the regression model obtained by considering data from expanding marshes are also reported. Names of individual study sites in legends are as follows: SB-East = eastern portions of the*

Saint-Brieuc marsh; SB-West = western portions of the Saint-Brieuc marsh; MSM = Mont Saint Michel; SW = The Swale; WS = The Wash; CM = Chongming; RD = Rudong.

Combined changes in both $\sum L$ and A_m are likely to affect marsh drainage density. However, our data highlight that the mean drainage distance (ℓ_m) remained fairly constant through time in all the studied marshes, each of which is characterized by a site-specific value of ℓ_m (Fig. 5 and Table 2). Significant changes in ℓ_m are only observed for MSM between 1965 and 1973 (Fig. 5b,g; see also Table 2) and SW between 20003 and 2005 (Fig. 5c,h; see also Table 2), that is, for the two study cases and periods in which marshes did not undergo significant lateral expansion, and active headward channel growth was observed. Increasing $\sum L$ due to headward erosion and relatively stable marsh area A_m thus led to pronounced decreases in ℓ_m and, therefore, to an increase in the overall marsh drainage density (δ). In contrast, both in MSM and SW, δ attained approximately constant values during periods characterized by active marsh expansion in the seaward direction, which is consistent with the temporal evolution of ℓ_m observed for all the other study sites (Fig. 5 and Table 2).

Hence, our results suggest that when marshes with stable landward boundaries expand seaward, tidal channel networks evolve in a fashion that tends to maintain the marsh drainage properties unaltered (Fig. 5). It thus appears that the mechanism of TCN geomorphological evolution in laterally expanding marshes tends to shape networks that are statistically self-similar to prior network configurations. Such a mechanism is different from previous observations carried out in tidal networks characterized by active headward channel erosion (Stefanon et al., 2010; Zhou et al., 2014b), wherein drainage properties of a given intertidal area were shown to vary considerably in time as $\sum L$ increased while A_m either remained approximately constant or reduced progressively due to marsh

lateral retreat. This is because most of the existing analyses of δ and ℓ_m focused on marshlands that were either characterized by stable spatial extent or experiencing marsh-area shrinking due to lateral erosion driven by, for example, the action of wind waves (e.g., Finotello et al., 2020; Leonardi et al., 2016; Tommasini et al., 2019).

Significant variations of δ and ℓ_m among different sites (Fig. 5 and Table 2) is likely due to site-specific tidal forcings and marsh-platform properties. Indeed, previous studies demonstrated that larger tidal prism are likely to produce TCNs with higher δ, and vice versa (Stefanon et al., 2012). Besides, modeling analyses suggested that TCNs in highly frictional salt-marsh platforms tend to develop fewer branches and are characterized by larger inter-channel distances and, therefore, by lower drainage density (Fagherazzi and Sun, 2004). In addition, morphological features of TCNs are also regulated by site-specific vegetation assemblages and animal activities, which critically affect flow turbulence and soil erosion across the marsh platform (Hughes et al., 2009; Schwarz et al., 2022; Temmerman et al., 2007). For example, sites where crab burrowing activity is more intense typically display higher δ due to the coupling of vegetation disappearance and reduction in local accretion, both aiding in reducing flow resistances and enhancing bottom shear stresses (Crotty et al., 2020; Escapa et al., 2007; Wilson et al., 2022). Besides, environmental changes, which can be significantly accelerated by human activities, can alternate vegetation distributions and biotic activities, thus possibly further modifying site-specific TCN morphological properties (Crotty et al., 2020; Finotello et al., 2022).

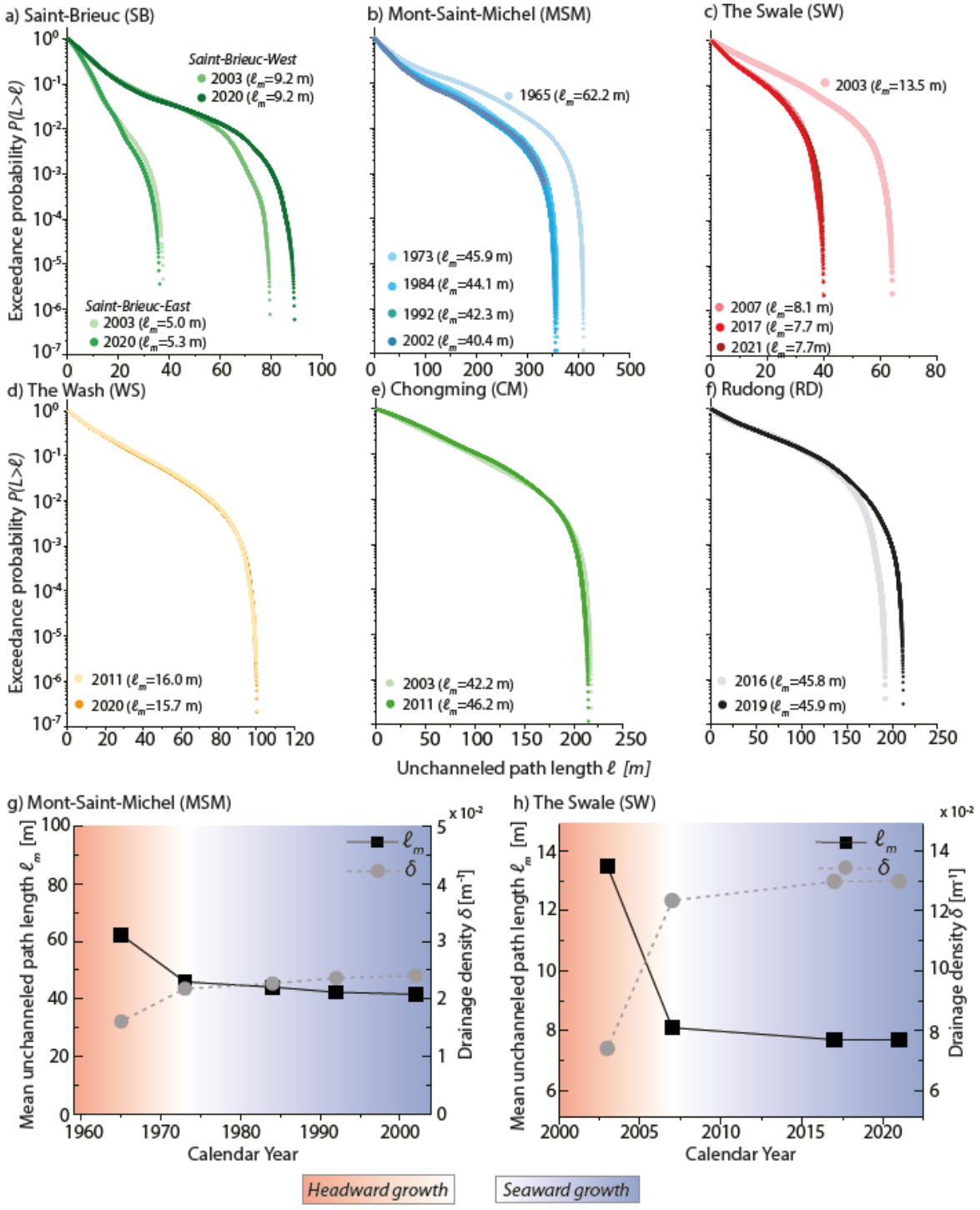

Fig. 5. *Evolution of tidal channel network morphometric features. (a,b,c,d,e,f) Empirical probability distributions of unchanneled path length (ℓ) computed by means of the simplified hydrodynamic model proposed by Rinaldo et al. (1999a, 1999b) are shown for each study case based on the exceedance probability $P(L > \ell)$. The latter is derived by computing L for every marsh site and*

plotting the probability obtained by counting the relative proportion of sites for which L exceeds a given value ℓ, here expressed in meters. In each panel, the mean unchanneled path length (ℓ_m) for different network configurations are also reported. (g,h) Evolution of the mean unchanneled path length (ℓ_m) and related drainage density ($\delta=\ell_m^{-1}$) in Mont-Saint-Michel and the Swale study cases. Different background colors highlight different evolution mechanisms of the coupled marsh-network system, with red denoting phases of network growth via headward erosion and blue emphasizing periods during which both marshes and channels expanded in the seaward direction.

Because concurrent headward channel growth and enhancement of drainage density appear to be unique to retreating or stable marshes, some explanation of why this behavior is absent from expanding marshes is warranted. In order to do so, we analyzed the distributions of maximum bottom shear stresses (τ_{max}) at channel tips based on equation (4), and compared them with realistic values of critical shear stress τ_c, that is the threshold shear stress required to initiate sediment motion. Based on literature data suggesting τ_c to typically range between 1 and 2 Pa over marsh platforms (Chen et al., 2011; D'Alpaos et al., 2005; Hir et al., 2008), we were able to estimate the number of actively eroding channel tips by considering three different values of τ_c equal to 1.0, 1.5 and 2.0 Pa. We focus in particular on the MSM (Figs .1b and 2g-l) and SW study cases (Figs. 1c and 3a-e), for which more than two aerial images were available, which allowed us to investigate the distributions of eroding tips during both periods of channel headward growth and marsh lateral expansion. Results show that the relative abundance of eroding tips (i.e., tips for which $\tau_{max}>\tau_c$) during the channel headward-growth phase (i.e., Fig. 6a for 1965 in MSM and Fig. 6b for 2003 in SW) is notably higher compared to periods when channels (and marshes) expand seaward (Fig. 6c-d). Hence, our data suggest that

seaward expansion of the coupled marsh-channel system significantly changes the hydrodynamics of intertidal plains, in this way effectively reducing bottom shear stresses at channel tips and limiting TCN landward expansion *via* headward growth. Thus, it emerges that marsh seaward expansion fundamentally changes the mechanism of TCN evolution from headward channel growth to seaward channel expansion, a shift that might represent an indicator of channel network adaptation to bio-morphodynamic processes in tidal landscapes.

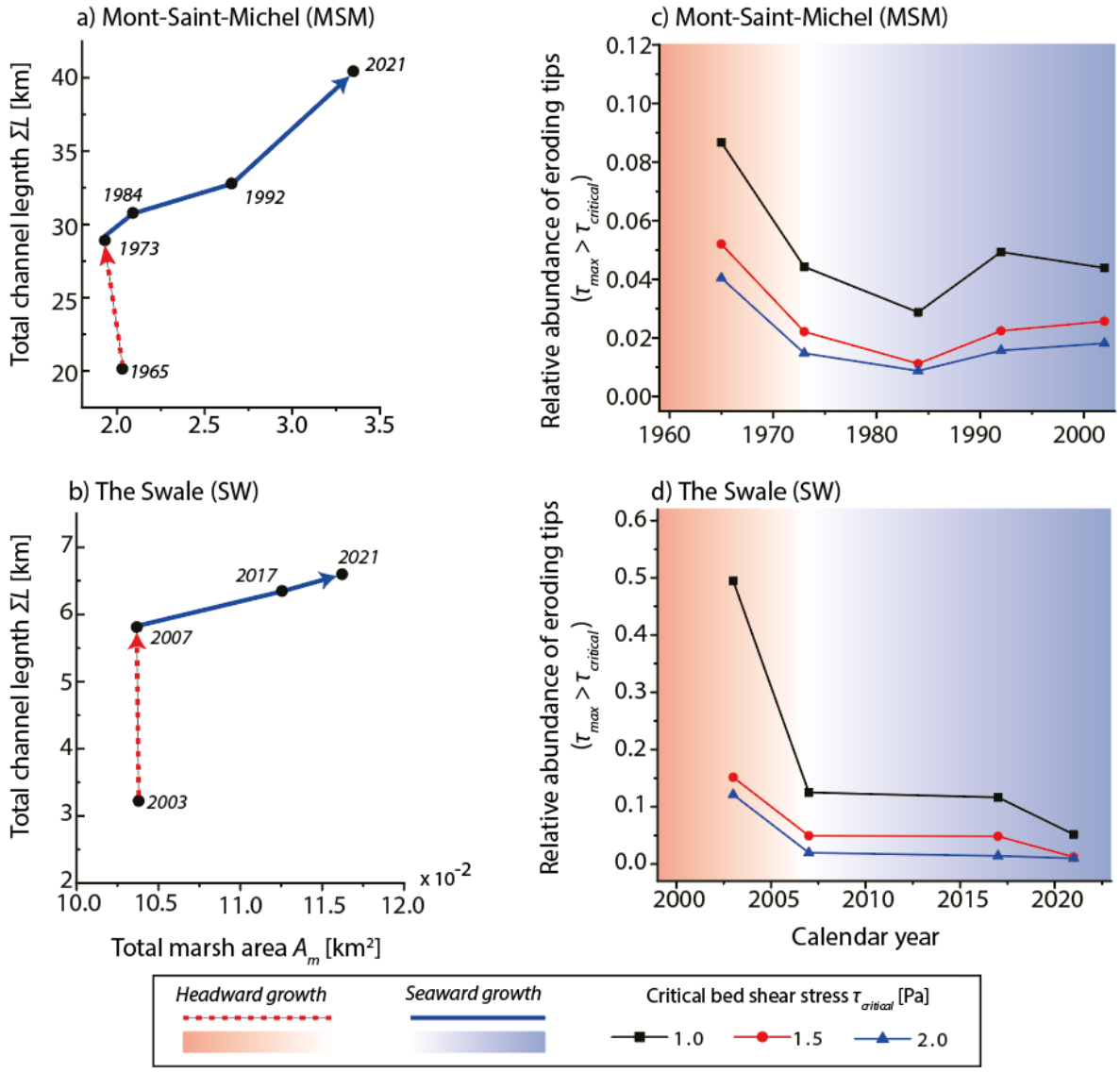

Fig 6. *Effects of changes in the evolution mechanisms of the coupled marsh-network system. (a,b) Evolution of total marsh area (A_m) vs. total channel length ($\sum L$) values in the marshes of Mont-Saint-Michelle and the Swale through time. (c,d) Changes in the relative abundance of eroding channel tips through time based on different values of critical shear stress for sediment erosion (τ_c). An eroding channel tip is identified as a channel head wherein $\tau_{max} > \tau_c$, being τ_{max} the maximum local bottom shear stress computed through the simplified hydrodynamic model proposed by Rinaldo et al. (1999a, 1999b). Red and blue background colors in each panel are used to identify different evolutionary phases of the coupled marsh-network system, with red denoting phases of network growth via headward erosion and blue emphasizing periods during which both marshes and channels expanded in the seaward direction.*

There are however some limitations in our approach that should be highlighted. First, the positions of marsh landward boundaries in all the studied marshes are fixed by the presence of man-made structures, which effectively prevents marsh landward migration and significantly impacts the distribution of τ_{max} by limiting flow velocities in the innermost marsh portions. Thus, it remains unclear whether the mechanisms of TCN evolution illustrated here, operate also in intertidal systems where landward marsh boundaries can change through time (Fagherazzi et al., 2019; Fitzgerald and Hughes, 2019; Kirwan and Gedan, 2019; Smith, 2013).

In addition, our analyses focused on a relatively narrow range of tidal wetlands, that is, on tidal marshes found in macro- and meso-tidal settings. Previous studies have demonstrated that these marshes are the most likely to receive enough mineral sediment supply to support marsh lateral

expansion (e.g., D'Alpaos et al., 2011; Ganju et al., 2017; Kirwan et al., 2016; Kirwan and Guntenspergen, 2010). Therefore, even though TCN evolution in microtidal settings is likely to follow mechanisms by all means similar to those we illustrated here, specific analyses will be needed to confirm such speculation.

Table 2. *Morphological features of TCN at each study site in different years. The type of marsh change from the corresponding date to the next observation, subdivided between prograding (P) and retreating (R), is also reported. (A_m: total channel area; $\sum L$: total channel length; A_c: total channel area; δ: drainage density; and ℓ_m=mean unchannelled path length).*

Study site	Year	A_m[km^2]	$\sum L$[km]	A_c[km^2]	δ[m]	ℓ_m[m]	Marsh change
SB-East	2003	0.053	2.953	2.00E-04	0.2	5	P
	2011	0.069	3.636	2.09E-04	0.189	5.3	--
SB-West	2003	0.311	13.803	4.05E-04	0.109	9.2	P
	2011	0.421	17.599	4.69E-04	0.109	9.2	--
MSM	1965	2.030	20.142	1.68E-01	0.016	62.2	R
	1973	1.930	28.903	8.93E-02	0.022	45.9	P
	1984	2.090	30.774	6.97E-02	0.023	44.1	P
	1992	2.653	32.788	2.40E-01	0.024	42.3	P
	2002	3.348	40.439	1.80E-01	0.025	40.4	--
SW	2003	0.104	3.222	2.42E-04	0.074	13.5	R
	2007	0.104	5.810	2.45E-04	0.123	8.1	P
	2017	0.113	6.349	2.40E-04	0.13	7.7	P
	2021	0.116	6.599	2.40E-04	0.13	7.7	--
WS	2011	0.999	30.610	5.20E-02	0.063	16	P
	2020	1.073	32.735	5.87E-02	0.064	15.7	--
CM	2003	3.958	43.058	2.55E-01	0.024	42.2	P
	2011	7.666	70.298	6.94E-01	0.022	46.2	--
RD	2016	0.665	7.503	2.50E-02	0.022	45.8	P
	2019	0.863	8.347	3.58E-02	0.022	45.9	--

4. Conclusions

We have analyzed the morphological evolution of several tidal channel networks found worldwide in salt-marsh systems characterized by active lateral expansion in the seaward direction. Thus, different from most empirical studies carried out so far, we investigated TCN evolution in salt marshes that are expanding rather than retreating, and wherein channels lengthen seaward instead of landward.

Seaward marsh expansion, which in our study cases is generally promoted by sufficient mineral sediment supply coupled with anthropogenically fixed position of marsh landward boundaries, led to a proportional increase in the overall marsh area and length of tidal channel networks. Moreover, in laterally-expanding marshes, tidal channel networks were shown to evolve primarily by seaward expansion, rather than by landward extension through the well-known headward-growth mechanism that typically operates in marsh systems that are either stable or retraining laterally.

This collectively leads to TCNs maintaining self-similar morphological structures in terms of drainage density. For the first time, we report such a self-similarity in TCNs, which has not been observed in marshes undergoing lateral erosion. By elucidating the evolutionary mechanisms of tidal channel networks in actively expanding salt marshes, our observations help to improve current knowledge on the morphodynamics of coupled TCN-marsh ecosystems, with direct practical implications for the conservation and restoration of coastal wetlands.

Author Contributions: Conception and design of the work: Z.Y., A.F., M.G., and A.D.A.; Data collection: Z.Y., G.G., C.G., S.M., B.T., D.L., C.S.; Data analysis and interpretation: Z.Y., A.F., A.D.A; Drafting article: Z.Y., A.F.; Critical revision of the article: all authors.

Conflict of interest: The authors declare that they have no known competing financial interests or personal relationships that could have appeared to influence the work reported in this paper.

Acknowledgment: This work was supported by the University of Padova SID2016 project titled "From channels to rock record: morphodynamic evolution of tidal meanders and related sedimentary products" (grant BIRD 168939 to Massimiliano Ghinassi), by the project HYDROSEM (Progetti di Eccellenza CARIPARO 2017, Cassa di Risparmio di Padova e Rovigo): "Fluvial and tidal meanders of the Venetian-Po plain: From hydrodynamics to stratigraphy" (PI Massimiliano Ghinassi), by the University of Padova Supporting TAlent in ReSearch (STARS) Grant entitled "TiDyLLy - Tidal network dynamics as drivers for ecomorphodynamics of low-lying coastal regions" (PI Alvise Finotello), and by the University of Padova SID2021 project "Unraveling Carbon Sequestration Potential by Salt-Marsh Ecosystems" (P.I. A. D'Alpaos). Z.Y. would like to thank the Fondazione Cariparo, for providing the essential funding for his Ph.D. study. Z.Y. also thanks Dr. Zeng Zhou for discussions regarding channel network evolution. We also thank the Editor and reviewers for their valuable suggestions and comments. We are grateful for constructive reviews from anonymous reviewers and the associate editor, which helped improve this paper.

Data availability: All the data are listed in the text, references, and figures.

References

Allen, J.R.L., 2000. Morphodynamics of Holocene salt marshes: A review sketch from the Atlantic and Southern North Sea coasts of Europe. Quat. Sci. Rev. 19, 1155–1231. https://doi.org/10.1016/S0277-3791(99)00034-7

Cahoon, D.R., French, J.R., Spencer, T., Reed, D., Möller, I., 2000. Vertical accretion versus elevational adjustment in UK saltmarshes: An evaluation of alternative methodologies. Geol. Soc. Spec. Publ. 175, 223–238. https://doi.org/10.1144/GSL.SP.2000.175.01.17

Chambers, R.M., Osgood, D.T., Bart, D.J., Montalto, F., 2003. Phragmites australis invasion and expansion in tidal wetlands: Interactions among salinity, sulfide, and hydrology. Estuaries 26, 398–406. https://doi.org/10.1007/BF02823716

Chen, C., Tian, B., Schwarz, C., Zhang, C., Guo, L., Xu, F., Zhou, Y., He, Q., 2021. Quantifying delta channel network changes with Landsat time-series data. J. Hydrol. 600, 126688. https://doi.org/10.1016/j.jhydrol.2021.126688

Chen, Y., Collins, M.B., Thompson, C.E.L., 2011. Creek enlargement in a low-energy degrading saltmarsh in southern England. Earth Surf. Process. Landforms 36, 767–778. https://doi.org/10.1002/esp.2104

Chen, Y., Thompson, C.E.L., Collins, M.B., 2012. Saltmarsh creek bank stability: Biostabilisation and consolidation with depth. Cont. Shelf Res. 35, 64–74. https://doi.org/10.1016/j.csr.2011.12.009

Cleveringa, J., Oost, A.P., 1999. The fractal geometry of tidal-channel systems in the Dutch Wadden Sea. Geol. en Mijnbouw/Netherlands J. Geosci. 78, 21–30. https://doi.org/10.1023/A:1003779015372

Coco, G., Zhou, Z., van Maanen, B., Olabarrieta, M., Tinoco, R., Townend, I., 2013. Morphodynamics of tidal networks: Advances and challenges. Mar. Geol. 346, 1–16. https://doi.org/10.1016/j.margeo.2013.08.005

Cosma, M., Finotello, A., Ielpi, A., Ventra, D., Oms, O., D'Alpaos, A., Ghinassi, M., 2020. Piracy-controlled geometry of tide-dominated point bars: Combined evidence from ancient sedimentary successions and modern channel networks. Geomorphology 370, 107402. https://doi.org/10.1016/j.geomorph.2020.107402

Crotty, S.M., Ortals, C., Pettengill, T.M., Shi, L., Olabarrieta, M., Joyce, M.A., Altieri, A.H., Morrison, E., Bianchi, T.S., Craft, C., Bertness, M.D., Angelini, C., 2020. Sea-level rise and the emergence of a

keystone grazer alter the geomorphic evolution and ecology of southeast US salt marshes. Proc. Natl. Acad. Sci. U. S. A. 117, 17891–17902. https://doi.org/10.1073/pnas.1917869117

D'Alpaos, A., Finotello, A., Goodwin, G.C.H., Mudd, S.M., 2021. Salt Marsh Hydrodynamics, in: FitzGerald, D., Hughes, Z. (Eds.), Salt Marshes. Cambridge University Press, Cambridge, pp. 53–81. https://doi.org/10.1017/9781316888933.005

D'Alpaos, A., Ghinassi, M., Finotello, A., Brivio, L., Bellucci, L.G., Marani, M., 2017. Tidal meander migration and dynamics: A case study from the Venice Lagoon. Mar. Pet. Geol. 87, 80–90. https://doi.org/10.1016/j.marpetgeo.2017.04.012

D'Alpaos, A., Lanzoni, S., Marani, M., Bonometto, A., Cecconi, G., Rinaldo, A., 2007. Spontaneous tidal network formation within a constructed salt marsh: Observations and morphodynamic modelling. Geomorphology 91, 186–197. https://doi.org/10.1016/j.geomorph.2007.04.013

D'Alpaos, A., Lanzoni, S., Marani, M., Fagherazzi, S., Rinaldo, A., 2005. Tidal network ontogeny: Channel initiation and early development. J. Geophys. Res. Earth Surf. 110, 1–14. https://doi.org/10.1029/2004JF000182

D'Alpaos, A., Mudd, S.M., Carniello, L., 2011. Dynamic response of marshes to perturbations in suspended sediment concentrations and rates of relative sea level rise. J. Geophys. Res. Earth Surf. 116, 1–13. https://doi.org/10.1029/2011JF002093

Desguée, R., Robin, N., Gluard, L., Monfort, O., Anthony, E.J., Levoy, F., 2011. Contribution of hydrodynamic conditions during shallow water stages to the sediment balance on a tidal flat: Mont-Saint-Michel Bay, Normandy, France. Estuar. Coast. Shelf Sci. 94, 343–354. https://doi.org/10.1016/j.ecss.2011.07.010

Détriché, S., Susperregui, A.S., Feunteun, E., Lefeuvre, J.C., Jigorel, A., 2011. Interannual (1999-2005) morphodynamic evolution of macro-tidal salt marshes in Mont-Saint-Michel Bay (France). Cont. Shelf Res. 31, 611–630. https://doi.org/10.1016/j.csr.2010.12.015

Escapa, M., Minkoff, D.R., Perillo, G.M.E., Iribarne, O., 2007. Direct and indirect effects of burrowing crab Chasmagnathus granulatus activities on erosion of southwest Atlantic Sarcocornia-dominated marshes. Limnol. Oceanogr. 52, 2340–2349. https://doi.org/10.4319/lo.2007.52.6.2340

Fagherazzi, S., Anisfeld, S.C., Blum, L.K., Long, E. V., Feagin, R.A., Fernandes, A., Kearney, W.S., Williams, K., 2019. Sea level rise and the dynamics of the marsh-upland boundary. Front. Environ. Sci. 7, 1–18. https://doi.org/10.3389/fenvs.2019.00025

Fagherazzi, S., Sun, T., 2004. A stochastic model for the formation of channel networks in tidal marshes. Geophys. Res. Lett. 31, 1–4. https://doi.org/10.1029/2004GL020965

Feola, A., Belluco, E., D'Alpaos, A., Lanzoni, S., Marani, M., Rinaldo, A., 2005. A geomorphic study of lagoonal landforms. Water Resour. Res. 41, 1–11. https://doi.org/10.1029/2004WR003811

Finotello, A., D'Alpaos, A., Marani, M., Bertuzzo, E., 2022. A Minimalist Model of Salt-Marsh Vegetation Dynamics Driven by Species Competition and Dispersal. Front. Mar. Sci. 9, 1–23. https://doi.org/10.3389/fmars.2022.866570

548 Finotello, A., Lanzoni, S., Ghinassi, M., Marani, M., Rinaldo, A., D'Alpaos, A., 2018. Field migration
549 rates of tidal meanders recapitulate fluvial morphodynamics. Proc. Natl. Acad. Sci. U. S. A. 115,
550 1463–1468. https://doi.org/10.1073/pnas.1711330115

551 Finotello, A., Lentsch, N., Paola, C., 2019. Experimental delta evolution in tidal environments:
552 Morphologic response to relative sea-level rise and net deposition. Earth Surf. Process. Landforms 44,
553 2000–2015. https://doi.org/10.1002/esp.4627

554 Finotello, A., Marani, M., Carniello, L., Pivato, M., Roner, M., Tommasini, L., D'alpaos, A., 2020.
555 Control of wind-wave power on morphological shape of salt marsh margins. Water Sci. Eng. 13, 45–
556 56. https://doi.org/10.1016/j.wse.2020.03.006

557 Fitzgerald, D.M., Hughes, Z., 2019. Marsh processes and their response to climate change and sea-
558 level rise. Annu. Rev. Earth Planet. Sci. 47, 481–517. https://doi.org/10.1146/annurev-earth-082517-
559 010255

560 Flint, J.J., 1973. Experimental development of headward growth of channel networks. Bull. Geol. Soc.
561 Am. 84, 1087–1094. https://doi.org/10.1130/0016-7606(1973)84<1087:EDOHGO>2.0.CO;2

562 Furgerot, L., Mouazé, D., Tessier, B., Perez, L., Haquin, S., Weill, P., Crave, A., 2016. Sediment
563 transport induced by tidal bores. An estimation from suspended matter measurements in the Sée River
564 (Mont-Saint-Michel Bay, northwestern France). Comptes Rendus - Geosci. 348, 432–441.
565 https://doi.org/10.1016/j.crte.2015.09.004

566 Ganju, N.K., Defne, Z., Kirwan, M.L., Fagherazzi, S., D'Alpaos, A., Carniello, L., 2017. Spatially
567 integrative metrics reveal hidden vulnerability of microtidal salt marshes. Nat. Commun. 8.
568 https://doi.org/10.1038/ncomms14156

569 Geng, L., D'Alpaos, A., Sgarabotto, A., Gong, Z., Lanzoni, S., 2021. Intertwined Eco-
570 Morphodynamic Evolution of Salt Marshes and Emerging Tidal Channel Networks. Water Resour.
571 Res. 57, 1–25. https://doi.org/10.1029/2021WR030840

572 Geng, L., Gong, Z., Zhou, Z., Lanzoni, S., D'Alpaos, A., 2020. Assessing the relative contributions of
573 the flood tide and the ebb tide to tidal channel network dynamics. Earth Surf. Process. Landforms 45,
574 237–250. https://doi.org/10.1002/esp.4727

575 Goodwin, G.C.H., Mudd, S.M., 2020. Detecting the morphology of prograding and retreating marsh
576 margins-example of a mega-tidal bay. Remote Sens. 12, 13. https://doi.org/10.3390/RS12010013

577 Goudie, A., 2013. Characterising the distribution and morphology of creeks and pans on salt marshes
578 in England and Wales using Google Earth. Estuar. Coast. Shelf Sci. 129, 112–123.
579 https://doi.org/10.1016/j.ecss.2013.05.015

580 Hir, P. Le, Cann, P., Waeles, B., Jestin, H., Bassoullet, P., 2008. Chapter 11 Erodibility of natural
581 sediments: experiments on sand/mud mixtures from laboratory and field erosion tests, in: Proceedings
582 in Marine Science. pp. 137–153. https://doi.org/10.1016/S1568-2692(08)80013-7

583 Hughes, Z.J., FitzGerald, D.M., Wilson, C.A., Pennings, S.C., Wiçski, K., Mahadevan, A., 2009.
584 Rapid headward erosion of marsh creeks in response to relative sea level rise. Geophys. Res. Lett. 36,
585 1–5. https://doi.org/10.1029/2008GL036000

586 Jarriel, T., Swartz, J., Passalacqua, P., 2021. Global rates and patterns of channel migration in river
587 deltas. Proc. Natl. Acad. Sci. U. S. A. 118. https://doi.org/10.1073/pnas.2103178118

588 Kalkan, K., Bayram, B., Maktav, D., Sunar, F., 2013. Comparison of support vector machine and
589 object based classification methods for coastline detection. Int. Arch. Photogramm. Remote Sens. Spat.
590 Inf. Sci. - ISPRS Arch. 40, 125–127. https://doi.org/10.5194/isprsarchives-XL-7-W2-125-2013

591 Kearney, W.S., Fagherazzi, S., 2016. Salt marsh vegetation promotes efficient tidal channel networks.
592 Nat. Commun. 7, 1–7. https://doi.org/10.1038/ncomms12287

593 Kerschnitzki, M., Kollmannsberger, P., Burghammer, M., Duda, G.N., Weinkamer, R., Wagermaier,
594 W., Fratzl, P., 2013. Architecture of the osteocyte network correlates with bone material quality. J.
595 Bone Miner. Res. 28, 1837–1845. https://doi.org/10.1002/jbmr.1927

596 Kirwan, M.L., Gedan, K.B., 2019. Sea-level driven land conversion and the formation of ghost forests.
597 Nat. Clim. Chang. 9, 450–457. https://doi.org/10.1038/s41558-019-0488-7

598 Kirwan, M.L., Guntenspergen, G.R., 2010. Influence of tidal range on the stability of coastal
599 marshland. J. Geophys. Res. Earth Surf. 115, 1–11. https://doi.org/10.1029/2009jf001400

600 Kirwan, M.L., Murray, A.B., Donnelly, J.P., Corbett, D.R., 2011. Rapid wetland expansion during
601 European settlement and its implication for marsh survival under modern sediment delivery rates.
602 Geology 39, 507–510. https://doi.org/10.1130/G31789.1

603 Kirwan, M.L., Temmerman, S., Skeehan, E.E., Guntenspergen, G.R., Fagherazzi, S., 2016.
604 Overestimation of marsh vulnerability to sea level rise. Nat. Clim. Chang. 6, 253–260.
605 https://doi.org/10.1038/nclimate2909

606 Kleinhans, M.G., Van Der Vegt, M., Terwisscha Van Scheltinga, R., Baar, A.W., Markies, H., 2012.
607 Turning the tide: Experimental creation of tidal channel networks and ebb deltas. Geol. en
608 Mijnbouw/Netherlands J. Geosci. 91, 311–323. https://doi.org/10.1017/S0016774600000469

609 Knighton, A.D., Mills, K., Woodroffe, C.D., 1991. Tidal-creek extension and salt water intrusion in
610 northern Australia. Geology 19, 831–834. https://doi.org/10.1130/0091-
611 7613(1991)019<0831:TCEASI>2.3.CO;2

612 Knighton, A.D., Woodroffe, C.D., Mills, K., 1992. The evolution of tidal creek networks, mary river,
613 northern Australia. Earth Surf. Process. Landforms 17, 167–190.
614 https://doi.org/10.1002/esp.3290170205

615 Ladd, C.J.T., Duggan-Edwards, M.F., Bouma, T.J., Pagès, J.F., Skov, M.W., 2019. Sediment Supply
616 Explains Long-Term and Large-Scale Patterns in Salt Marsh Lateral Expansion and Erosion. Geophys.
617 Res. Lett. 46, 11178–11187. https://doi.org/10.1029/2019GL083315

618 Lentsch, N., Finotello, A., Paola, C., 2018. Reduction of deltaic channel mobility by tidal action under
619 rising relative sea level. Geology 46, 599–602. https://doi.org/10.1130/G45087.1

Leonardi, N., Ganju, N.K., Fagherazzi, S., 2016. A linear relationship between wave power and erosion determines salt-marsh resilience to violent storms and hurricanes. Proc. Natl. Acad. Sci. U. S. A. 113, 64–68. https://doi.org/10.1073/pnas.1510095112

Leopold, L.B., Collins, J.N., Collins, L.M., 1993. Hydrology of some tidal channels in estuarine marshland near San Francisco. Catena 20, 469–493. https://doi.org/10.1016/0341-8162(93)90043-O

Levoy, F., Anthony, E.J., Dronkers, J., Monfort, O., Izabel, G., Larsonneur, C., 2017. Influence of the 18.6-year lunar nodal tidal cycle on tidal flats: Mont-Saint-Michel Bay, France. Mar. Geol. 387, 108–113. https://doi.org/10.1016/j.margeo.2017.03.009

Levoy, F., Anthony, E.J., Monfort, O., Larsonneur, C., 2000. The morphodynamics of megatidal beaches in Normandy, France. Mar. Geol. 171, 39–59. https://doi.org/10.1016/S0025-3227(00)00110-9

Li, R., Yu, Q., Wang, Y., Wang, Z.B., Gao, S., Flemming, B., 2018. The relationship between inundation duration and Spartina alterniflora growth along the Jiangsu coast, China. Estuar. Coast. Shelf Sci. 213, 305–313. https://doi.org/10.1016/j.ecss.2018.08.027

Marani, M., Belluco, E., D'Alpaos, A., Defina, A., Lanzoni, S., Rinaldo, A., 2003. On the drainage density of tidal networks. Water Resour. Res. 39, 1–11. https://doi.org/10.1029/2001WR001051

May, M.K., 2002. Pattern and Process of Headward Erosion in Salt Marsh Tidal Creeks. East Carolina University.

Ni, W., Wang, Y.P., Symonds, A.M., Collins, M.B., 2014. Intertidal flat development in response to controlled embankment retreat: Freiston Shore, The Wash, UK. Mar. Geol. 355, 260–273. https://doi.org/10.1016/j.margeo.2014.06.001

Norris, K., Cook, T., O'Dowd, B., Durdin, C., 1997. The Density of Redshank Tringa totanus Breeding on the Salt-Marshes of the Wash in Relation to Habitat and Its Grazing Management. J. Appl. Ecol. 34, 999. https://doi.org/10.2307/2405289

Ponsero, A.., Le Mao, P.., Sou, P.Y.É.., Allain, J.., Vidal, J.., 2009. Ecosystem quality and natural heritage preservation: The case of the littoral eutrophica-tion and the wintering of Brent Geese Branta b. bernicla in the bay of Saint-Brieuc (France). Rev. d'Ecologie (La Terre la Vie) 64, 157–170.

Pye, K., 1995. Controls on long-term saltmarsh accretion and erosion in the Wash, eastern England. J. Coast. Res. 11, 337–356.

Rankey, E.C., Morgan, J., 2002. Quantified rates of geomorphic change on a modern carbonate tidal flat, Bahamas. Geology 30, 583–586. https://doi.org/10.1130/0091-7613(2002)030<0583:QROGCO>2.0.CO;2

Rinaldo, A., Fagherazzi, S., Lanzoni, S., Marani, M., Dietrich, W.E., 1999a. Tidal networks 2. Watershed delineation and comparative network morphology. Water Resour. Res. 35, 3905–3917. https://doi.org/10.1029/1999WR900237

Rinaldo, A., Fagherazzi, S., Lanzoni, S., Marani, M., Dietrich, W.E., 1999b. Tidal networks 3. Landscape-forming discharges and studies in empirical geomorphic relationships. Water Resour. Res. 35, 3919–3929. https://doi.org/10.1029/1999WR900238

Roner, M., Ghinassi, M., Finotello, A., Bertini, A., Combourieu-Nebout, N., Donnici, S., Gilli, A., Vannacci, M., Vigliotti, L., Bellucci, L.G., Fedi, M., Liccioli, L., Tommasini, L., D'Alpaos, A., 2021. Detecting the Delayed Signatures of Changing Sediment Supply in Salt-Marsh Landscapes: The Case of the Venice Lagoon (Italy). Front. Mar. Sci. 8. https://doi.org/10.3389/fmars.2021.742603

Sanderson, E.W., Foin, T.C., Ustin, S.L., 2001. A simple empirical model of salt marsh plant spatial distributions with respect to a tidal channel network. Ecol. Modell. 139, 293–307. https://doi.org/10.1016/S0304-3800(01)00253-8

Sanderson, E.W., Ustin, S.L., Foin, T.C., 2000. The influence of tidal channels on the distribution of salt marsh plant species in Petaluma Marsh, CA, USA. Plant Ecol. 146, 29–41. https://doi.org/10.1023/A:1009882110988

Schwarz, C., van Rees, F., Xie, D., Kleinhans, M.G., van Maanen, B., 2022. Salt marshes create more extensive channel networks than mangroves. Nat. Commun. 13, 1–9. https://doi.org/10.1038/s41467-022-29654-1

Shi, B.W., Yang, S.L., Wang, Y.P., Bouma, T.J., Zhu, Q., 2012. Relating accretion and erosion at an exposed tidal wetland to the bottom shear stress of combined current-wave action. Geomorphology 138, 380–389. https://doi.org/10.1016/j.geomorph.2011.10.004

Shi, Z., Lamb, H.F., Collin, R.L., 1995. Geomorphic change of saltmarsh tidal creek networks in the Dyfi Estuary, Wales. Mar. Geol. 128, 73–83. https://doi.org/10.1016/0025-3227(95)00074-9

Smith, J.A.M., 2013. The Role of Phragmites australis in Mediating Inland Salt Marsh Migration in a Mid-Atlantic Estuary. PLoS One 8. https://doi.org/10.1371/journal.pone.0065091

Stefanon, L., Carniello, L., D'Alpaos, A., Lanzoni, S., 2010. Experimental analysis of tidal network growth and development. Cont. Shelf Res., The Coastal Morphodynamics of Venice Lagoon and its Inlets 30, 950–962. https://doi.org/10.1016/j.csr.2009.08.018

Stefanon, L., Carniello, L., D'Alpaos, A., Rinaldo, A., 2012. Signatures of sea level changes on tidal geomorphology: Experiments on network incision and retreat. Geophys. Res. Lett. 39, 1–6. https://doi.org/10.1029/2012GL051953

Sturbois, A., Cormy, G., Schaal, G., Gauthier, O., Ponsero, A., Le Mao, P., Riera, P., Desroy, N., 2021. Characterizing spatio-temporal changes in benthic communities: Taxonomic and functional trajectories of intertidal assemblages in the bay of Saint-Brieuc (English Channel). Estuar. Coast. Shelf Sci. 262, 107603. https://doi.org/10.1016/j.ecss.2021.107603

Sturbois, A., Riera, P., Desroy, N., Brébant, T., Carpentier, A., Ponsero, A., Schaal, G., 2022. Spatio-temporal patterns in stable isotope composition of a benthic intertidal food web reveal limited influence from salt marsh vegetation and green tide. Mar. Environ. Res. 175, 105572. https://doi.org/10.1016/j.marenvres.2022.105572

692 Temmerman, S., Bouma, T.J., Van de Koppel, J., Van der Wal, D., De Vries, M.B., Herman, P.M.J.,
693 2007. Vegetation causes channel erosion in a tidal landscape. Geology 35, 631–634.
694 https://doi.org/10.1130/G23502A.1

695 Tessier, B., Billeaud, I., Sorrel, P., Delsinne, N., Lesueur, P., 2012. Infilling stratigraphy of macrotidal
696 tide-dominated estuaries. Controlling mechanisms: Sea-level fluctuations, bedrock morphology,
697 sediment supply and climate changes (The examples of the Seine estuary and the Mont-Saint-Michel
698 Bay, English Channel, NW Fr. Sediment. Geol. 279, 62–73.
699 https://doi.org/10.1016/j.sedgeo.2011.02.003

700 Tommasini, L., Carniello, L., Ghinassi, M., Roner, M., D'Alpaos, A., 2019. Changes in the wind-
701 wave field and related salt-marsh lateral erosion: inferences from the evolution of the Venice Lagoon
702 in the last four centuries. Earth Surf. Process. Landforms 44, 1633–1646.
703 https://doi.org/10.1002/esp.4599

704 Tucker, G.E., Catani, F., Rinaldo, A., Bras, R.L., 2001. Statistical analysis of drainage density from
705 digital terrain data. Geomorphology 36, 187–202. https://doi.org/10.1016/S0169-555X(00)00056-8

706 Van Maanen, B., Coco, G., Bryan, K.R., 2015. On the ecogeomorphological feedbacks that control
707 tidal channel network evolution in a sandy mangrove setting. Proc. R. Soc. A Math. Phys. Eng. Sci.
708 471, 20150115. https://doi.org/10.1098/rspa.2015.0115

709 Vandenbruwaene, W., Meire, P., Temmerman, S., 2012. Formation and evolution of a tidal channel
710 network within a constructed tidal marsh. Geomorphology 151–152, 114–125.
711 https://doi.org/10.1016/j.geomorph.2012.01.022

712 Vlaswinkel, B.M., Cantelli, A., 2011. Geometric characteristics and evolution of a tidal channel
713 network in experimental setting. Earth Surf. Process. Landforms 36, 739–752.
714 https://doi.org/10.1002/esp.2099

715 Wang, Y.P., Gao, S., Jia, J., Thompson, C.E.L., Gao, J., Yang, Y., 2012. Sediment transport over an
716 accretional intertidal flat with influences of reclamation, Jiangsu coast, China. Mar. Geol. 291–294,
717 147–161. https://doi.org/10.1016/j.margeo.2011.01.004

718 Willemsen, P.W.J.M., Smits, B.P., Borsje, B.W., Herman, P.M.J., Dijkstra, J.T., Bouma, T.J., Hulscher,
719 S.J.M.H., 2022. Modeling Decadal Salt Marsh Development: Variability of the Salt Marsh Edge
720 Under Influence of Waves and Sediment Availability. Water Resour. Res. 58, e2020WR028962.
721 https://doi.org/10.1029/2020WR028962

722 Wilson, C.A., Hughes, Z.J., FitzGerald, D.M., 2022. Causal relationships among sea level rise, marsh
723 crab activity, and salt marsh geomorphology. Proc. Natl. Acad. Sci. U. S. A. 119, e2111535119.
724 https://doi.org/10.1073/pnas.2111535119

725 Yang, P., Hu, Z., Shu, Q., 2021. Factors affecting soil organic carbon content between natural and
726 reclaimed sites in rudong coast, jiangsu province, china. J. Mar. Sci. Eng. 9.
727 https://doi.org/10.3390/jmse9121453

728 Yang, S.L., Luo, X., Temmerman, S., Kirwan, M.L., Bouma, T., Xu, K., Zhang, S., Fan, J., Shi, B.,
729 Yang, H., Wang, Y.P., Shi, X., Gao, S., 2020. Role of delta-front erosion in sustaining salt marshes

730 under sea-level rise and fluvial sediment decline. Limnol. Oceanogr. 65, 1990–2009.
731 https://doi.org/10.1002/lno.11432

732 Yang, S.L., Milliman, J.D., Li, P., Xu, K., 2011. 50,000 dams later: Erosion of the Yangtze River and
733 its delta. Glob. Planet. Change 75, 14–20. https://doi.org/10.1016/j.gloplacha.2010.09.006

734 Yang, S.L., Zhang, J., Zhu, J., Smith, J.P., Dai, S.B., Gao, A., Li, P., 2005. Impact of dams on Yangtze
735 River sediment supply to the sea and delta intertidal wetland response. J. Geophys. Res. Earth Surf.
736 110, F03006. https://doi.org/10.1029/2004JF000271

737 Zhao, L.X., Xu, C., Ge, Z.M., Van De Koppel, J., Liu, Q.X., 2019. The shaping role of self-
738 organization: Linking vegetation patterning, plant traits and ecosystem functioning. Proc. R. Soc. B
739 Biol. Sci. 286. https://doi.org/10.1098/rspb.2018.2859

740 Zheng, Z., Zhou, Y., Tian, B., Ding, X., 2016. The spatial relationship between salt marsh vegetation
741 patterns, soil elevation and tidal channels using remote sensing at Chongming Dongtan Nature
742 Reserve, China. Acta Oceanol. Sin. 35, 26–34. https://doi.org/10.1007/s13131-016-0831-z

743 Zhou, Z., Olabarrieta, M., Stefanon, L., D'Alpaos, A., Carniello, L., Coco, G., 2014a. A comparative
744 study of physical and numerical modeling of tidal network ontogeny. J. Geophys. Res. Earth Surf. 119,
745 892–912. https://doi.org/10.1002/2014JF003092

746 Zhou, Z., Stefanon, L., Olabarrieta, M., D'Alpaos, A., Carniello, L., Coco, G., 2014b. Analysis of the
747 drainage density of experimental and modelled tidal networks. Earth Surf. Dyn. 2, 105–116.
748 https://doi.org/10.5194/esurf-2-105-2014

749